

Optimization methods for achieving high diffraction efficiency with perfect electric conducting gratings

Rubén Aylwin¹, Gerardo Silva-Oelker², Carlos Jerez-Hanckes³, and Patrick Fay⁴

¹*Department of Electrical Engineering, Pontificia Universidad Católica de Chile, Santiago, Chile.*

²*Department of Mechanical Engineering, Universidad Tecnológica Metropolitana, Santiago, Chile.*

³*Faculty of Engineering and Sciences, Universidad Adolfo Ibáñez, Santiago, Chile.*

⁴*Department of Electrical Engineering, University of Notre Dame, IN, USA.*

April 7, 2020

Abstract

This work presents the implementation, analysis, and convergence study of first- and second-order optimization methods applied to one-dimensional periodic gratings. Through boundary integral equations and shape derivatives, the profile of a grating (taken to be a perfect electric conductor) is optimized such that it maximizes the diffraction efficiency for a given diffraction mode. We provide a thorough comparison of two optimization methods: a first-order one based on gradient descent and a second-order approach based on Newton iteration. For the latter, two variations have been explored; in one option, the first Newton method replaces the usual Newton step for the absolute values of the spectral decomposition of the Hessian matrix to deal with non-convexity, while in the second, a modified version of this Newton method is considered to reduce computational time required to compute the Hessian. Numerical examples are provided to validate our claims.

1 Introduction

One-dimensional gratings are able to diffract, split, reflect and transmit light, depending on geometrical parameters such as amplitude, period, and shape. For example, it is well known that metallic gratings exhibit Wood’s anomalies [53, 38] and cavity resonances [37]. Of particular interest in applications is the diffraction efficiency—defined as the amount of power diffracted in one mode [35]. Due to these properties, gratings have several applications in science and engineering, ranging from X-ray spectroscopy [29], energy conversion devices such as photovoltaics [47] and thermophotovoltaics [45], beam splitters [13], quantum cascade lasers [14], and filters [32], to name a few. Consequently, a large body of literature has been devoted to the study of physical phenomena [25, 18, 28], mathematical modeling [9, 56, 22, 44], fabrication [27, 19, 41], and optimization of gratings.

Among the optimization methods for designing gratings, genetic algorithms and particle swarm optimization have been studied and implemented for applications such as energy conversion [43, 10] and filters [42]. These methods have shown to be practical options due to their simplicity and flexibility in implementation. However, the aforementioned techniques suffer from disadvantages such as partial convergence and the need for a large number of evaluations of the cost function. In contrast, methods that rely on following the gradient direction to minimize a suitable cost function can be more appropriate for some problems. Roger [40], for instance, studied the optimization of a

perfect electric conducting (PEC) grating by the steepest-descent and conjugate-gradient methods along with boundary integral equations (BIE). Recently, Bao et al. [5] implemented the Landweber iteration also along with BIE for inverse problems, showing the applicability of gradient optimization. Methods based on so-called *shape derivatives* have been theoretically proposed [16, 17] for optimization and successfully applied to the design of devices [33]. However, grating geometry optimization using shape derivatives, to the best of our knowledge, has not been explored yet. This work aims to provide details and examples of first- and second-order methods based on shape gradients for PEC grating profile optimization.

The use of optimization algorithms can lead to non-trivial grating shapes (e.g., échelle or holographic). Fortunately, suitable fabrication approaches for such profiles are currently available, including electron beam lithography [55, 49], laser ablation [3], deposition techniques [51] as well as nanoimprint techniques [54, 21]. Additionally, intricate structures [1, 52] can now be manufactured, thereby increasing the range of shape possibilities and making it possible to design and fabricate optimum gratings.

In this work, we implemented and compared first- and second-order optimization algorithms to maximize the diffraction efficiency. Diffraction efficiency was chosen as the target figure of merit for its importance in applications [8]. In our approach, the wave scattering model problem in computational volume is reduced to one defined on the grating boundary through an integral formulation and a suitable quasi-periodic Green's function. Optimization is carried out by minimizing or maximizing a cost or objective function using first- and second-order shape gradients [11] of the defined far-field operator, which maps the grating profile to the diffraction field components. In the case of the first-order method, it is shown that the shape derivative approach is equivalent to the work presented by Roger [40]. However, due to the fact that this optimization problem can be highly non-convex, additional techniques are explored to improved performance. In this regard, two Newton-based second-order algorithms are implemented and studied. First, a second-order method with a modified step, as proposed by [12], to deal with the non-convexity is considered. Then, this algorithm is further improved to reduce the computational time required to compute second derivatives (Hessian matrix). Numerical results show that, as expected, second-order algorithms converge quadratically. Moreover, these methods reduce both the computation time and the number of iterations required to find a maximum, as well as the ability to escape from saddle points. These results pave the way for more efficient approaches of grating optimization, and periodic structures in general. Furthermore, the studied techniques can also be applied to inverse design problems.

The rest of the paper is organized as follows. In Section 2, the wave scattering by a grating problem is presented, along with the boundary integral formulation and the definition of diffraction efficiency. Section 3 describes the optimization methods: shape derivatives are introduced and first- and second-order methods are detailed. Numerical examples are provided in Section 4, analyzing the impact of different parameters (e.g., wavelength, angle of incidence, etc.). Finally, conclusions are drawn in Section 5.

2 Scattering Problem and Boundary Integral Formulation

A PEC grating with period Λ and surface given by $\tilde{\Gamma} \times \mathbb{R}$ is considered (Fig. 1). The domain $\tilde{D} \times \mathbb{R} \subset \mathbb{R}^3$ is defined as the open region of propagation above the grating surface, assumed to be free space and characterized by its impedance $\eta = \sqrt{\mu/\varepsilon}$, where ε and μ correspond to the permittivity and permeability of vacuum, respectively.

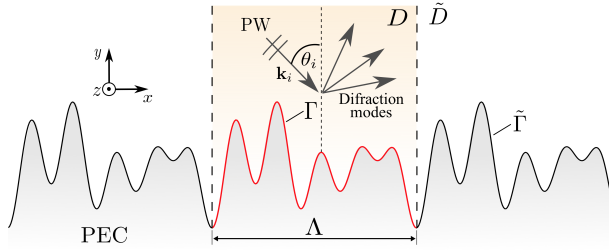


Figure 1: Graphic description of grating parameters. The figure shows a perfectly conducting grating with a period Λ . The domain, D , above the grating and its surface, $\tilde{\Gamma}$, are also shown. Both D and Γ are defined in one period (orange region and red line, respectively).

2.1 Scattering Problem

The scattering of a monochromatic plane wave (PW) with wave vector \mathbf{k}_i by a grating surface described in Fig. 1 is considered. Furthermore, we assume the wave vector to be such that it has no z component ($\mathbf{k}_i = (k_x, k_y)$), so that Maxwell's equations may be decomposed into transverse electric (TE) and transverse magnetic (TM) polarizations (see [6] and references therein). For brevity, only TE polarization ($E_x = E_y = H_z = 0$) is considered in this study. Nevertheless, optimization for TM polarization follows the same approach with different boundary conditions. Hence, this work focuses on finding the z component of the electric field, defined as:

$$u(\mathbf{r}) = E_z(\mathbf{r}), \quad \mathbf{r} \in \tilde{D}, \quad (1)$$

where $\mathbf{r} := (x, y) \in \mathbb{R}^2$ is the position vector. Then, the total field u satisfies the Helmholtz equation

$$\Delta u + k^2 u = 0 \quad \text{in} \quad \tilde{D}, \quad (2)$$

$$u = 0 \quad \text{on} \quad \tilde{\Gamma}, \quad (3)$$

where $k := \omega/c$ is the wavenumber. As previously stated, we consider the scattering of an incident plane wave (PW in Fig. 1)

$$u^i(\mathbf{r}) := E_0 e^{i\mathbf{k}_i \cdot \mathbf{r}} \quad \forall \mathbf{r} \in \tilde{D},$$

onto the grating surface $\tilde{\Gamma}$, where $\mathbf{k}_i = (k_x, k_y) = k(\sin \theta_i, \cos \theta_i)$ is the incident wave vector (with angle of incidence θ_i and null z component), and $E_0 > 0$ corresponds to the amplitude of the incident electric field. By linearity, the total field, u , is $u = u^i + u^s$, where u^s is the scattered field. Since plane waves satisfy (2), we may restate the previous system as a problem for the scattered field as follows:

$$\Delta u^s + k^2 u^s = 0 \quad \text{in} \quad \tilde{D}, \quad (4)$$

$$u^s = -u^i \quad \text{on} \quad \tilde{\Gamma}. \quad (5)$$

The periodicity of the grating and the quasi-periodicity of u^i , i.e.

$$u^i(x + n\Lambda, y) = u^i(x, y) e^{i k_x \Lambda n}, \quad \forall n \in \mathbb{Z}, \quad (6)$$

enable us to restate the problem for the scattered field over one cell of the periodic domain \tilde{D} . However, the problem still lacks appropriate radiation conditions at infinity, which, for the sake of brevity, will not be derived here. Instead, we refer to [6, 30, 23] and references therein for a

derivation (and discussion) of the appropriate radiation conditions in periodic problems. For a fixed $d \in \mathbb{R}$, such that $\tilde{\Gamma}$ lies strictly below the line $y = d$ (Fig. 1), we define the following domains:

$$D := \{\mathbf{r} \in \tilde{D} : x \in (0, \Lambda)\} \quad \text{and} \quad D_d := \{\mathbf{r} \in D : y < d\}.$$

Analogously, we define the grating surface over one period

$$\Gamma := \{\mathbf{r} \in \tilde{\Gamma} : x \in (0, \Lambda)\}.$$

Additionally, the Sobolev space of integrable functions with integrable first-order derivatives on D_d that satisfy (6) is denoted $H_{k_x; \Lambda}^1(D_d)$. We then seek to find a field $u^s \in H_{k_x; \Lambda}^1(D_d)$ that solves

$$\begin{aligned} \Delta u^s + k^2 u^s &= 0 \quad \text{in } D_H, \\ u^s &= -u^i =: g \quad \text{on } \Gamma, \\ u^s(x, y) &= \sum_{n \in \mathbb{Z}} u_n(d) e^{i(k_{y,n}(y-d) + k_{x,n}x)} \quad \forall y \geq d, \end{aligned} \tag{7}$$

where, for each $n \in \mathbb{Z}$, $k_{x,n} := k \sin \theta_i + 2\pi n / \Lambda$ and

$$k_{y,n} := \begin{cases} \sqrt{k^2 - k_{x,n}^2} & \text{if } k^2 \geq k_{x,n}^2 \\ i\sqrt{k_{x,n}^2 - k^2} & \text{if } k^2 < k_{x,n}^2 \end{cases}.$$

The last line in (7) corresponds to the radiation condition for the periodic domain, also known as the Rayleigh expansion for u^s [6, 35, 23]. In order to avoid Rayleigh anomalies, we further assume that no $n \in \mathbb{Z}$ exists such that $k_{x,n}^2 = k^2$.

2.2 Boundary Integral Equations

To find the scattered field, u^s , we use BIEs (particularly the electric field integral equation), motivated by the unboundedness of the domain D . Therefore, the representation ansatz for u^s :

$$u^s(\mathbf{r}) = (\mathbf{SL}j)(\mathbf{r}), \quad \mathbf{r} \in D, \tag{8}$$

where j is an unknown surface density (in this case, the surface current density) and \mathbf{SL} is the quasi-periodic single-layer operator, whose action on the density j may be represented through the quasi-periodic Green's function G^p as

$$(\mathbf{SL}j)(\mathbf{r}) := ik\eta \int_{\Gamma} G^p(\mathbf{r}, \mathbf{r}') j(\mathbf{r}') d\Gamma(\mathbf{r}'), \quad \mathbf{r} \in D. \tag{9}$$

Using (8), (9), and the boundary conditions in (7), the BIE for the unknown surface density j may be written as:

$$\mathcal{V}j = -u^i \quad \text{on } \Gamma, \tag{10}$$

where \mathcal{V} is the boundary integral operator mapping the surface density j to the boundary values of $\mathbf{SL}j$. The quasi-periodic Green's function, G^p , is given by [26, 50]

$$G^p(\mathbf{r}, \mathbf{r}') = \frac{i}{2\Lambda} \sum_{n=-\infty}^{\infty} \frac{e^{i(k_{x,n}(x-x') + i k_{y,n}|y-y'|)}}{k_{y,n}}. \tag{11}$$

2.3 The Scattered Far-Field

As displayed in (7), the scattered field may be decomposed as a linear combination of complex exponentials. Of these, only those corresponding to $n \in \mathbb{Z}$ such that $k^2 > k_{x,n}^2$ do not decay as y grows to infinity. Therefore, the scattered far-field depends solely on the Rayleigh coefficients corresponding to a real value for $k_{y,n}$, i.e., on $\{u_n(d)\}_{n \in \mathcal{N}(k, \theta_i, \Lambda)}$ where

$$\mathcal{N}(k, \theta_i, \Lambda) := \{n \in \mathbb{Z} : k > |k \sin(\theta_i) + 2\pi n / \Lambda|\}.$$

The coefficients of the Rayleigh expansion in the radiation condition of Eq. (7) may be extracted from the scattered field as follows:

$$u_n(d) = \frac{1}{\Lambda} \int_0^\Lambda u^s(x, d) e^{-ik_{x,n}x} dx = -e^{ik_{y,n}d} \frac{k\eta}{2\Lambda k_{y,n}} \int_{\Gamma} j(\mathbf{r}) e^{-i\mathbf{K}_n \cdot \mathbf{r}} d\Gamma(\mathbf{r}), \quad (12)$$

where $\mathbf{K}_n := (k_{x,n}, k_{y,n})$. Then, the associated grating diffraction efficiency can be computed through $e_n := \frac{k_{y,n}}{k_y} |u_n(d)|^2$, further justifying the choice to employ BIE to solve the scattering problem.

3 Optimization

As stated in the introduction, we aim to find optimal grating profiles in the sense that they maximize (or minimize) functions of the diffraction efficiencies, e.g.,

$$\max_{\Gamma} e_n(\Gamma), \quad \min_{\Gamma} \sum_{n \in \mathcal{N}'} (e_n(\Gamma) - e_n^{\text{obj}})^2,$$

for some $\mathcal{N}' \subseteq \mathcal{N}(k, \theta_i, \Lambda)$ and some objective efficiency e_n^{obj} in the case of minimization. With this in mind, we turn to the problem of computing derivatives of the far-field Rayleigh coefficients as functions of the grating geometry for the implementation of local search optimization algorithms. To do so, we introduce the n -th mode far-field operator as

$$\mathcal{F}_n : \Gamma \mapsto u_n. \quad (13)$$

This operator maps a grating profile Γ to $\mathcal{F}_n(\Gamma) = u_n$, the n -th coefficient of the Rayleigh expansion of the diffracted field. Henceforth, we assume k , Λ , and θ_i to be fixed.

3.1 Shape Calculus and Shape Derivatives

To compute derivatives of the far-field operator with respect to the grating geometry, we use tools from shape calculus [36, 46]. For $m \in \mathbb{N}$ and a given grating profile Γ of class C^m (the m -th derivative exists and is continuous), we introduce the following space of periodic functions:

$$C_p^\ell(\Gamma) := \left\{ \tau \in C^\ell(\Gamma; \mathbb{R}^2) : \tau \text{ is periodic} \right\},$$

for any non-negative integer $\ell \leq m$. Moreover, for any $a \in C_p^0(\Gamma)$, we introduce the perturbed grating profile as

$$\Gamma_a := \{\mathbf{r} + a(\mathbf{r}) : \mathbf{r} \in \Gamma\}.$$

Then, the definition of the shape derivative of \mathcal{F}_n at Γ in the direction a is

$$\mathcal{F}'_n(\Gamma; a) := \lim_{\epsilon \rightarrow 0} \frac{1}{\epsilon} (\mathcal{F}_n(\Gamma_{\epsilon a}) - \mathcal{F}_n(\Gamma)), \quad (14)$$

whenever the limit in the right hand side of (14) exists [24, 23, 36, 46]. The computation of $\mathcal{F}'_n(\Gamma; a)$, for a in $C_p^2(\Gamma)$, can be performed by solving a problem analogous to (7) through the use of the following relation:

$$\mathcal{F}'_n(\Gamma; a) = \mathcal{F}_n(u'[a]),$$

where $u'[a]$ is the unique solution in $H_{k_x; \Lambda}^1(D_d)$ to the following scattering problem:

$$\begin{aligned} \Delta u'[a] + k^2 u'[a] &= 0 \quad \text{in } D_d, \\ u'[a] &= -(a \cdot \nu) \frac{\partial}{\partial \nu} u \quad \text{on } \Gamma, \\ u'[a](\mathbf{r}) &= \sum_{n \in \mathbb{Z}} u'_n[a](d) e^{i(k_{y,n}(y-d) + k_{x,n}x)} \quad \forall y \geq d, \end{aligned}$$

where ν is the normal vector to Γ . This result follows by modifying the proof of Theorem 2.1 in [24] to the quasi-periodic setting (cf. [2]).

Since we are interested in analyzing second-order optimization methods, we also introduce second-order shape derivatives. The second-order shape derivative of \mathcal{F}_n at Γ in the directions $a_1, a_2 \in C_p(\Gamma)$ is defined as

$$\mathcal{F}''_n(\Gamma; a_1; a_2) := \lim_{\epsilon \rightarrow 0} \frac{1}{\epsilon} (\mathcal{F}'_n(\Gamma_{\epsilon a_2}; a_1 \circ \psi_\epsilon) - \mathcal{F}'_n(\Gamma; a_1)), \quad (15)$$

with

$$\psi_\epsilon := \phi_\epsilon^{-1}, \quad \phi_\epsilon := \begin{cases} \Gamma & \rightarrow \Gamma_{\epsilon a_2} \\ \mathbf{r} & \mapsto \mathbf{r} + \epsilon a_2(\mathbf{r}) \end{cases}.$$

This definition was introduced in the context of scattering from bounded obstacles in [20]. Analogously to the case of first-order shape derivatives, the computation of $\mathcal{F}''_n(\Gamma; a_1; a_2)$, for a_1 and a_2 in $C_p^3(\Gamma)$, follows from:

$$\mathcal{F}''_n(\Gamma; a_1; a_2) = \mathcal{F}_n(u''[a_1; a_2]),$$

where $u''[a_1; a_2]$ is the unique solution in $H_{k_x; \Lambda}^1(D_d)$ to the following scattering problem:

$$\begin{aligned} \Delta u''[a_1, a_2] + k^2 u''[a_1, a_2] &= 0 \quad \text{in } D_d, \\ u''[a_1, a_2] &= -(a_1 \cdot \nu) \frac{\partial u'[a_2]}{\partial \nu} - (a_2 \cdot \nu) \frac{\partial u'[a_1]}{\partial \nu} \\ &\quad + ((a_1 \cdot \nu)(a_2 \cdot \nu) - (a_1 \cdot \tau)(a_2 \cdot \tau)) \kappa \frac{\partial u}{\partial \nu} \\ &\quad + ((a_1 \cdot \tau)(\tau \cdot \nabla(a_2 \cdot \nu)) + (a_2 \cdot \tau)(\tau \cdot \nabla(a_1 \cdot \nu))) \frac{\partial u}{\partial \nu} \quad \text{on } \Gamma, \quad \text{and} \\ u''[a_1, a_2](\mathbf{r}) &= \sum_{n \in \mathbb{Z}} u''_n[a_1; a_2](d) e^{i(k_{y,n}(y-d) + k_{x,n}x)} \quad \forall y \geq d, \end{aligned}$$

where ν , τ , and κ are the normal vector, the tangent vector, and the curvature of Γ , respectively.

Throughout the following sections, we consider, without loss of generality, $\Lambda = 1$. Moreover, we assume Γ to be given as follows,

$$\Gamma := \left\{ \mathbf{r} \in \mathbb{R}^2 : y = \sum_{\ell=1}^N \mathcal{A}_\ell \sin(2\pi\ell x) + \mathcal{B}_\ell \cos(2\pi\ell x), x \in (0, 1) \right\}.$$

Then, $\mathcal{F}_n(\Gamma) = \mathcal{F}_n(\mathcal{A}_1, \mathcal{B}_1, \dots, \mathcal{A}_N, \mathcal{B}_N)$ and the optimization problem is now finite dimensional on the $2N$ variables $\{\mathcal{A}_\ell\}_{\ell=1}^N$ and $\{\mathcal{B}_\ell\}_{\ell=1}^N$. It holds that

$$\frac{\partial \mathcal{F}_n}{\partial \mathcal{A}_\ell} = \mathcal{F}'_n(\Gamma; \sin(2\pi\ell x)) \quad \text{and} \quad \frac{\partial \mathcal{F}_n}{\partial \mathcal{B}_\ell} = \mathcal{F}'_n(\Gamma; \cos(2\pi\ell x)).$$

Note that $\sin(2\pi\ell x)$ and $\cos(2\pi\ell x)$ represent directions. This means that $2N$ problems need to be solved to compute every required derivative. Analogous relations can be found for the second-order derivatives of \mathcal{F}_n .

3.2 Adjoint Method for the Computation of Shape Derivatives

The computation of each derivative of $\mathcal{F}_n(\mathcal{A}_1, \mathcal{B}_1, \dots, \mathcal{A}_N, \mathcal{B}_N)$ requires solving a boundary integral equation with a varying right-hand side. The same holds for each second-order derivative, which also requires the computation of boundary data of first-order shape derivatives. We may achieve the computation of derivatives more efficiently through the adjoint method [48], considering the integral in (12) as a duality product and denoting $g_n(\mathbf{r}) := e^{-i\mathbf{K}_n \cdot \mathbf{r}}$, which yields

$$\langle j, g_n \rangle_\Gamma = \langle \mathcal{V}^{-1}(g), g_n \rangle_\Gamma = \left\langle \mathcal{V}^{-\top}(g_n), g \right\rangle_\Gamma.$$

Hence, if j^{adj} is a surface density such that it solves the following integral equation:

$$\mathcal{V}^\top j^{\text{adj}} = g_n, \tag{16}$$

then, we may compute shape derivatives in the direction $a \in C_p^2(\Gamma)$ as:

$$\mathcal{F}'_n(\Gamma; a) = \left\langle j^{\text{adj}}, -(a \cdot \nu) j \right\rangle_\Gamma. \tag{17}$$

According to (17), all of the first-order derivatives can be computed by solving two boundary integral equations of the form of (10) and then computing the specified integral. In (16), \mathcal{V}^\top is the boundary integral operator analogous to \mathcal{V} for the adjoint quasi-periodic Green's function given by

$$G_{\text{adj}}^p(\mathbf{r}, \mathbf{r}') = \frac{i}{2\Lambda} \sum_{n=-\infty}^{\infty} \frac{e^{i\tilde{k}_{x,n}(x-x') + ik_{y,n}|y-y'|}}{k_{y,n}},$$

where $\tilde{k}_{x,n} := -k \sin(\theta_i) + n$ for all $n \in \mathbb{N}$. The same formula for the first-order shape derivatives of the far-field operator was found in [39] through the use of reciprocity relations between solutions of scattering problems. Analogously,

$$\mathcal{F}''_n(\Gamma; a_1; a_2) = \left\langle j^{\text{adj}}, u''[a_1, a_2]|_\Gamma \right\rangle_\Gamma. \tag{18}$$

3.3 First-Order Optimization

Throughout this and the following subsection (concerning a second-order optimization algorithm) we consider the optimization problem of minimizing a function $f : \mathbb{R}^{2N} \rightarrow \mathbb{R}$ such that

$$f(\mathcal{A}_1, \mathcal{B}_1, \dots, \mathcal{A}_N, \mathcal{B}_N) = \tilde{f}(e_n(\mathcal{A}_1, \mathcal{B}_1, \dots, \mathcal{A}_N, \mathcal{B}_N))$$

for a smooth function $\tilde{f} : \mathbb{R} \rightarrow \mathbb{R}$ (e.g., $\tilde{f}(x) = x$, $\tilde{f}(x) = -x$ or $\tilde{f}(x) = (x - c)^2$ for some $c \in \mathbb{R}$). Hence, our optimization problem may be stated as

$$\min_{\mathbf{x} \in \mathcal{O}_{\text{ad}}} f(\mathbf{x}) = \min_{\Gamma \in \mathcal{O}_{\text{ad}}^S} \tilde{f}(e_n(\Gamma)),$$

where \mathcal{O}_{ad} is a set of admissible shape parameters and $\mathcal{O}_{\text{ad}}^S$ is the set of admissible boundaries Γ such that each $\mathbf{x} \in \mathcal{O}_{\text{ad}}$ determines exactly one $\Gamma \in \mathcal{O}_{\text{ad}}^S$. Notice that first-order shape derivatives of the grating efficiency may be computed as

$$e'_n(\Gamma; a) = \frac{2k_{y,n}}{k_y} (\text{Re}(\mathcal{F}_n(\Gamma))\text{Re}(\mathcal{F}'_n(\Gamma; a)) + \text{Im}(\mathcal{F}_n(\Gamma))\text{Im}(\mathcal{F}'_n(\Gamma; a))). \quad (19)$$

Given (17) and (19), first-order derivatives of the objective function can be computed, requiring the solution of only two integral equations and $2N$ independent integrals (which may be computed in parallel). For an initial set-up of the geometry given by $\mathbb{R}^{2N} \ni \mathbf{x}^{(0)} := (\mathcal{A}_1^{(0)}, \mathcal{B}_1^{(0)}, \dots, \mathcal{A}_N^{(0)}, \mathcal{B}_N^{(0)})$, we will consider the usual first-order optimization algorithm

$$\mathbf{x}^{(t)} = \mathbf{x}^{(t-1)} - h \nabla f(\mathbf{x}^{(t-1)}),$$

where $h > 0$ is the step size of the method, which may be backtracked at each step so that it varies at each iteration. The interested reader may refer to [15, 31] for details.

3.4 Second-Order Optimization

Local search algorithms based on the computation of gradients, such as the one described in Section 3.3 above, while being simple and ensuring convergence to local optima, suffer from a number of disadvantages. These include their inability to differentiate between local and global optima; their need for a large number of iterations for the algorithm to converge; the fact that they may get stuck in saddle points—points satisfying first-order optimality conditions but not second-order ones. When the objective function is known to be convex, Newton methods are the preferred choice of algorithm—at least whenever the computation of the Hessian matrix is not prohibitively expensive. As before, (18) allows us to approximate second derivatives of the far field through solving $2N$ additional integral equations, while second-order derivatives for the diffraction efficiency are computed as

$$\begin{aligned} e''_n(\Gamma; a_1; a_2) = & \frac{2k_{y,n}}{k_y} (\text{Re}(\mathcal{F}'_n(\Gamma; a_1))\text{Re}(\mathcal{F}'_n(\Gamma; a_2)) + \text{Im}(\mathcal{F}'_n(\Gamma; a_1))\text{Im}(\mathcal{F}'_n(\Gamma; a_2)) \\ & + \text{Re}(\mathcal{F}_n(\Gamma))\text{Re}(\mathcal{F}''_n(\Gamma; a_1; a_2)) + \text{Im}(\mathcal{F}_n(\Gamma))\text{Im}(\mathcal{F}''_n(\Gamma; a_1; a_2))). \end{aligned}$$

Since we cannot expect our objective function to be convex, we turn to a modified version of Newton's algorithm for non-convex functions [34, 12] that replaces the usual Newton step $\Delta \mathbf{x} := H(\mathbf{x})\nabla f(\mathbf{x})$ with the modified step $\Delta \mathbf{x} := |H(\mathbf{x})|\nabla f(\mathbf{x})$, where $H(\mathbf{x})$ is the Hessian matrix of $f(\mathbf{x})$ and $|H(\mathbf{x})|$ is the matrix resulting from taking the spectral decomposition of $H(\mathbf{x})$ and replacing all

its negative eigenvalues by their absolute value. The modified Newton iteration is therefore given as

$$\mathbf{x}^{(t)} = \mathbf{x}^{(t-1)} - h|H(\mathbf{x}^{(t-1)})|\nabla f(\mathbf{x}^{(t-1)}). \quad (20)$$

A variant of the algorithm (second-order- H in Figs. 3 and 4) recalculates $|H|$ every $m \in \mathbb{N}$ iterations, i.e.,

$$\mathbf{x}^{(t \cdot m + i)} = \mathbf{x}^{(t \cdot m + i - 1)} - h|H(\mathbf{x}^{(t \cdot m)})|\nabla f(\mathbf{x}^{(t \cdot m + i - 1)}), \quad (21)$$

for $i = \{1, \dots, m\}$ and $k \in \mathbb{N}_0$, which proves to be advantageous to reduce the computational burden associated with computing the Hessian matrix. Both alternatives will be implemented and compared. We observe that our proposed modified Newton step results in a more rapid escape from saddle points than for the usual gradient step and ensures a faster convergence rate in the directions of eigenvectors associated with positive eigenvalues (see Theorem 3.2 in [34] and the accompanying discussion).

4 Numerical Examples

In this section, a number of numerical examples comparing the proposed first and second-order methods are presented. A standard Galerkin formulation with piecewise polynomials of degree one was employed to numerically solve the required boundary integral equations (previously used by the authors in [44]). All computations were performed on a AMD Opteron 6386 SE server, where parallelization was only used to assemble the relevant matrices.

We give our conclusions and recommendations (based on our numerical experiments) in the following section.

4.1 Quadratic Convergence to Local Optima

To show some of the advantages of the chosen second-order optimization method, in this section we illustrate its convergence properties by presenting examples that exhibit quadratic convergence to local optima. To do so, results of two different optimization cases are analyzed (Fig. 2 (a) and (b)). Their optimization is based on an objective function of the form:

$$\tilde{f}(e_n(\Gamma)) = \left(e_n(\Gamma) - e_n^{\text{obj}} \right)^2, \quad (22)$$

which we attempt to minimize for different $n \in \mathbb{N}$ and $e_n^{\text{obj}} \in [0, 1]$. In these cases, a step-size $h = 1$ is suitable for our modified Newton method (and no backtracking of h is required to decrease our objective function). We take a number of steps of gradient descent from a randomized initial geometry and focus on examples for which both the first- and second-order algorithms find optimal geometries Γ_{obj} such that

$$\tilde{f}(e_n(\Gamma_{\text{obj}})) = 0.$$

Examples when this optimization fails to happen behave similarly as those presented in the following section; these will be discussed later in Section 4.2. The parameters for each optimization set up are indicated in Fig. 2, which also shows the value of the objective function of both algorithms and specifies the convergence rate of the optimization variables for the last iterations of the modified

Newton method. The convergence rate, q , of the series of steps $\{\mathbf{x}^t\}_{t \in \mathbb{N}}$ is estimated through the formula

$$q \approx \frac{\log \left(\frac{\|\mathbf{x}^{(t+3)} - \mathbf{x}^{(t+2)}\|}{\|\mathbf{x}^{(t+2)} - \mathbf{x}^{(t+1)}\|} \right)}{\log \left(\frac{\|\mathbf{x}^{(t+2)} - \mathbf{x}^{(t+1)}\|}{\|\mathbf{x}^{(t+1)} - \mathbf{x}^{(t)}\|} \right)}.$$

As expected, both examples exhibit a rate of convergence ≈ 2 . The accelerated convergence is also displayed by the images in Figure 2 and we remark that both methods converge to the same optimal geometries. We stress that the results in this section have the purpose of displaying the convergence properties of the modified Newton method for objective functions as in (22), rather than comparing the efficiency between the algorithms (which we do in the next section).

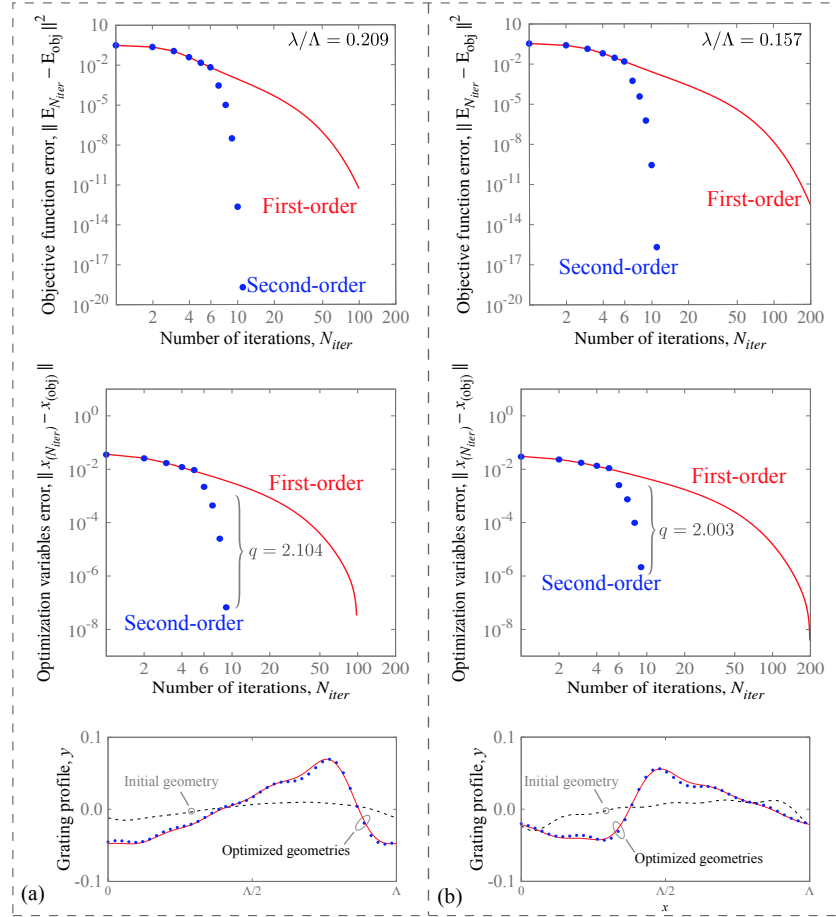


Figure 2: Two examples of optimization for objective functions as in (22). The objective function error (top panels), optimization variable error (middle panels), and initial and optimized geometries (bottom panels) are shown. Example (a) optimizes the grating profile for the $n = -1$ diffraction order to an objective efficiency of 60% for an incidence angle of $\theta_i = \pi/6$ and (b) optimizes the profile for the $n = 1$ diffraction order to an objective efficiency of 65% for an incidence angle of $\theta_i = \pi/4$. The first 6 iterations of the modified Newton method correspond to first-order iterations. Additionally, the quadratic rate of convergence is shown, $q = 2.104$ for example (a) and $q = 2.003$ for example (b).

4.2 Efficiency Maximization

We now focus on maximizing objective functions of the form

$$\tilde{f}(e_n(\Gamma)) = e_n(\Gamma) \quad (23)$$

for different $n \in \mathbb{N}$ and compare, as before, two different examples with the objective of comparing the number of iterations both methods require to converge to optimal geometries. From [34, 12], we expect the iteration count of the modified Newton method to be lower than that for the first-order method. We compare two versions of the modified Newton method (those in (20) and (21) with $m = 2$) to the first-order method. The step-size is backtracked at each iteration using a line search [7] and Armijo-Goldstein condition, i.e., for $\alpha \in (0, \frac{1}{2})$ and $\beta \in (0, 1)$, a step in direction \mathbf{p} and size h is accepted only if

$$f(\mathbf{x} + h\mathbf{p}) > f(\mathbf{x}) + \beta(h\mathbf{p} \cdot \nabla f(\mathbf{x})).$$

If the step is rejected, h is decreased to αh . So that the comparison is as fair as possible, the same parameters for the backtracking are chosen for all methods ($\alpha = 0.2$ and $\beta = 0.5$ for both examples). The algorithms stop if either the gradient of the objective function or the step-size at any given iteration falls beneath a certain tolerance. We note that in this case, due to the non-convexity of $e_n(\Gamma)$, quadratic convergence was not observed. Figures 3 and 4 display the diffraction efficiency of the target mode being optimized at each iteration for all three methods, the time each method took to arrive at a tolerance $\varepsilon_{tol} = 10^{-3}$ from the maximum efficiency attained, and the final optimized geometries. We note that, generally, more than one computation of the objective function (which requires the solution of a linear system) was required for the step size backtracking, so the time each method takes to achieve its optimum is not strictly proportional to the number of iterations. Both versions of the Newton method maximize the objective function more rapidly than the gradient method (with respect to iteration count). Moreover, the computational time required for both of the second-order- H algorithms is significantly smaller than for the first-order method.

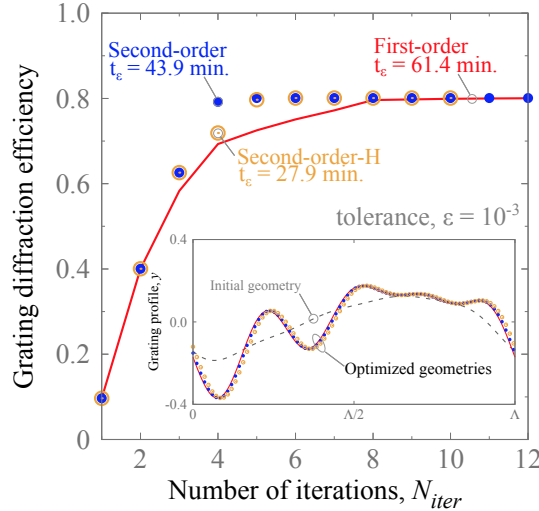


Figure 3: Grating diffraction maximization is shown for the three studied optimization methods, first-order (red line), second-order (blue-filled circles), and modified second-order (orange circles). The parameters are $\theta = \frac{5}{36}\pi$, $k = 20$, $n = 1$, and $N = 4$. The inset shows the initial (\mathbf{x}^0) and optimized geometries.

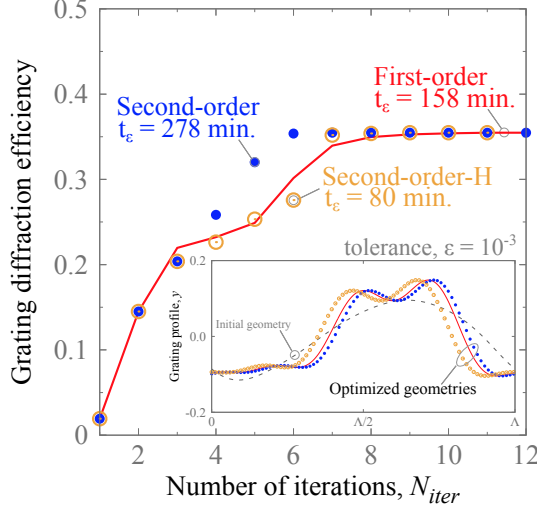


Figure 4: Grating diffraction maximization is shown for the three studied optimization methods, first-order (red line), second-order (blue-filled circles), and modified second-order (orange circles). The parameters are $\theta = \frac{1}{4}\pi$, $k = 30$, $n = -1$, and $N = 4$. The inset shows the initial (\mathbf{x}^0) and optimized geometries.

5 Conclusions

This work analyzed and compared a first-order algorithm, as well as two second-order algorithms presented in [34, 12] to a shape optimization problem of PEC periodic gratings as applied to the practical challenge of optimizing diffraction efficiency. First and second-order derivatives were computed following [46, 36] for shape derivatives and [24, 20] for first and second-order optimization methods.

The modified second-order method for non-convex functions proved to (i) achieve quadratic convergence of the optimization variables for the objective function in (22) and (ii) converge to optimal geometries in a lower iteration count than first-order methods for the maximization of grating efficiencies, even if second-order convergence rate is not observed. Furthermore, the observed quadratic convergence in the first two numerical examples seems to be a consequence of the quadratic nature of the objective function in (22), hinting that—when such behavior is expected—the modified Newton method should prove advantageous. In particular, applications of inverse problems employ objective functions that should behave in a similar manner near their optima (see [4] and references therein).

The variant of the analyzed second-order method that recomputes $|H|$ every $m > 1$ iterations (rather than at each iteration), while increasing the number of steps required to converge, proved to be more efficient than its counterpart ($m = 1$). This alternative mitigates the computational cost of computing the Hessian matrix at each iteration, while still retaining enough of its properties to be advantageous. In particular, numerical examples showed that this version of the modified Newton method (second-order- H) was always faster than the gradient method, both in iteration count and computational time.

Funding

This work was supported, in part, by Conicyt-PFCHA/Doctorado Nacional/2017-21171791. C Jerez-Hanckes work was sponsored by Fondecyt Regular 1171491.

References

- [1] Mukti Aryal, Doo-Hyun Ko, John R. Tumbleston, Abay Gadisa, Edward T. Samulski, and Rene Lopez. Large area nanofabrication of butterfly wings three dimensional ultrastructures. *Journal of Vacuum Science & Technology B, Nanotechnology and Microelectronics: Materials, Processing, Measurement, and Phenomena*, 30(6):061802, November 2012.
- [2] Rubén Aylwin, Carlos Jerez-Hanckes, and José Pinto. On the properties of quasi-periodic boundary integral operators for the helmholtz equation. *Integral Equations and Operator Theory*, 92(2), March 2020.
- [3] Mark Andreas Bader, Christoph Kappel, André Selle, Jürgen Ihlemann, Mi Li Ng, and Peter R. Herman. F₂-laser-machined submicrometer gratings in thin dielectric films for resonant grating waveguide applications. *Applied Optics*, 45(25):6586, September 2006.
- [4] Gang Bao and David C Dobson. Modeling and optimal design of diffractive optical structures. *Surveys on Mathematics for Industry*, 8(1):37–62, 1998.
- [5] Gang Bao, Peijun Li, and Junliang Lv. Numerical solution of an inverse diffraction grating problem from phaseless data. *Journal of the Optical Society of America A*, 30(3):293, February 2013.
- [6] Anne-Sophie Bonnet-Bendhia and Felipe Starling. Guided waves by electromagnetic gratings and non-uniqueness examples for the diffraction problem. *Mathematical Methods in the Applied Sciences*, 17(5):305–338, 1994.
- [7] Stephen Boyd and Lieven Vandenberghe. *Convex Optimization*. Cambridge University Press, USA, 2004.
- [8] A. Bunkowski, O. Burmeister, T. Clausnitzer, E.-B. Kley, A. Tünnermann, K. Danzmann, and R. Schnabel. Optical characterization of ultrahigh diffraction efficiency gratings. *Appl. Opt.*, 45(23):5795–5799, Aug 2006.
- [9] Simon N. Chandler-Wilde, Chris R. Ross, and B. O. Zhang. Scattering by infinite one-dimensional rough surfaces. *Proceedings of the Royal Society A: Mathematical, Physical and Engineering Sciences*, 455(1990):3767–3787, 1999.
- [10] Y. B. Chen and K. H. Tan. The profile optimization of periodic nano-structures for wavelength-selective thermophovoltaic emitters. *International Journal of Heat and Mass Transfer*, 53(23–24):5542–5551, 2010.
- [11] Martin Costabel and Frédérique Le Louër. Shape derivatives of boundary integral operators in electromagnetic scattering. part i: Shape differentiability of pseudo-homogeneous boundary integral operators. *Integral Equations and Operator Theory*, 72(4):509–535, Apr 2012.

- [12] Yann N Dauphin, Razvan Pascanu, Caglar Gulcehre, Kyunghyun Cho, Surya Ganguli, and Yoshua Bengio. Identifying and attacking the saddle point problem in high-dimensional non-convex optimization. In *Advances in neural information processing systems*, pages 2933–2941, 2014.
- [13] Jeffrey A. Davis, Jingo Adachi, Carlos R. Fernández-Pousa, and Ignacio Moreno. Polarization beam splitters using polarization diffraction gratings. *Optics Letters*, 26(9):587, May 2001.
- [14] Afusat O. Dirusu, Claire F. Gmachl, and Deborah L. Sivco. Sub-wavelength antireflection gratings on quantum cascade lasers. In Carmen Mermelstein and David P. Bour, editors, *Novel In-Plane Semiconductor Lasers VI*. SPIE, February 2007.
- [15] Ross Drummond and Stephen Duncan. Accelerated gradient methods with memory. *arXiv preprint arXiv:1805.09077*, 2018.
- [16] K. Eppler and H. Harbrecht. Second-order shape optimization using wavelet BEM. *Optimization Methods and Software*, 21(1):135–153, February 2006.
- [17] Karsten Eppler. Boundary integral representations of second derivatives in shape optimization. *Discussiones Mathematicae. Differential Inclusions, Control and Optimization*, 20(1):63, 2012.
- [18] Noah Graham. Casimir energies of periodic dielectric gratings. *Physical Review A - Atomic, Molecular, and Optical Physics*, 90(3), 2014.
- [19] A E Grigorescu and C W Hagen. Resists for sub-20-nm electron beam lithography with a focus on HSQ: state of the art. *Nanotechnology*, 20(29):292001, July 2009.
- [20] Frank Hettlich and William Rundell. A second degree method for nonlinear inverse problems. *SIAM Journal on Numerical Analysis*, 37(2):587–620, 1999.
- [21] Hiroaki Honma, Masato Mitsudome, Shintaro Itoh, Makoto Ishida, Kazuaki Sawada, and Kazuhiro Takahashi. Fabrication of free-standing subwavelength metal–insulator–metal gratings using high-aspect-ratio nanoimprint techniques. *Japanese Journal of Applied Physics*, 55(6S1):06GP20, May 2016.
- [22] Guanghui Hu and Andreas Rathsfeld. Scattering of time-harmonic electromagnetic plane waves by perfectly conducting diffraction gratings. *IMA Journal of Applied Mathematics (Institute of Mathematics and Its Applications)*, 80(2):508–532, 2015.
- [23] Andreas Kirsch. Diffraction by periodic structures. In *Inverse problems in mathematical physics*, pages 87–102. Springer, 1993.
- [24] ANDREAS Kirsch. The domain derivative and two applications in inverse scattering theory. *Inverse problems*, 9(1):81, 1993.
- [25] Yuzhang Liang, Wei Peng, Rui Hu, and Helin Zou. Extraordinary optical transmission based on subwavelength metallic grating with ellipse walls. *Optics Express*, 21(5):6139, 2013.
- [26] C.M. Linton. *Journal of Engineering Mathematics*, 33(4):377–401, 1998.
- [27] C. Lu and R.H. Lipson. Interference lithography: a powerful tool for fabricating periodic structures. *Laser & Photonics Reviews*, 4(4):568–580, May 2009.

- [28] A A Maradudin, I Simonsen, J Polanco, and R M Fitzgerald. Rayleigh and wood anomalies in the diffraction of light from a perfectly conducting reflection grating. *Journal of Optics*, 18(2):024004, January 2016.
- [29] Randall McEntaffer, Casey DeRoo, Ted Schultz, Brennan Gantner, James Tutt, Andrew Holland, Stephen O'Dell, Jessica Gaskin, Jeffrey Kolodziejczak, William W. Zhang, Kai-Wing Chan, Michael Biskach, Ryan McClelland, Dmitri Iazikov, Xinpeng Wang, and Larry Koecher. First results from a next-generation off-plane x-ray diffraction grating. *Experimental Astronomy*, 36(1-2):389–405, May 2013.
- [30] Jean-Claude Nedelec and Felipe Starling. Integral equation methods in a quasi-periodic diffraction problem for the time-harmonic maxwell's equations. *SIAM Journal on Mathematical Analysis*, 22(6):1679–1701, 1991.
- [31] Yurii Nesterov. *Lectures on convex optimization*, volume 137. Springer, 2018.
- [32] Manoj Niraula, Jae Woong Yoon, and Robert Magnusson. Mode-coupling mechanisms of resonant transmission filters. *Optics Express*, 22(21):25817, October 2014.
- [33] A. Paganini, S. Sargheini, R. Hiptmair, and Ch. Hafner. Shape optimization of microlenses. *Optics Express*, 23(10):13099, 2015.
- [34] Santiago Paternain, Aryan Mokhtari, and Alejandro Ribeiro. A newton-based method for nonconvex optimization with fast evasion of saddle points. *SIAM Journal on Optimization*, 29(1):343–368, January 2019.
- [35] Roger Petit, editor. *Electromagnetic Theory of Gratings*. Springer Berlin Heidelberg, 1980.
- [36] Oliver Pironneau, editor. *Optimal Shape Design for Elliptic Systems*. Springer Berlin Heidelberg, 1984.
- [37] Giorgio Quaranta, Guillaume Basset, Olivier J. F. Martin, and Benjamin Gallinet. Recent advances in resonant waveguide gratings. *Laser & Photonics Reviews*, 12(9):1800017, July 2018.
- [38] L. Rayleigh. On the dynamical theory of gratings. *Proceedings of the Royal Society A: Mathematical, Physical and Engineering Sciences*, 79(532):399–416, August 1907.
- [39] A Roger. Generalized reciprocity relations for perfectly conducting gratings. *Optica Acta: International Journal of Optics*, 29(10):1427–1439, 1982.
- [40] A. Roger. Optimization of perfectly conducting gratings a general method. *Optica Acta: International Journal of Optics*, 30(3):387–398, March 1983.
- [41] Muhammad Rizwan Saleem, Rizwan Ali, Mohammad Bilal Khan, Seppo Honkanen, and Jari Turunen. Impact of atomic layer deposition to nanophotonic structures and devices. *Frontiers in Materials*, 1, October 2014.
- [42] Mehrdad Shokooh-Saremi and Robert Magnusson. Particle swarm optimization and its application to the design of diffraction grating filters. *Optics Letters*, 32(8):894, March 2007.
- [43] G. Silva-Oelker, C. Jerez-Hanckes, and P. Fay. High-temperature tungsten-hafnia optimized selective thermal emitters for thermophotovoltaic applications. *Journal of Quantitative Spectroscopy and Radiative Transfer*, 231:61–68, July 2019.

- [44] Gerardo Silva-Oelker, Ruben Aylwin, Carlos Jerez-Hanckes, and Patrick Fay. Quantifying the impact of random surface perturbations on reflective gratings. *IEEE Transactions on Antennas and Propagation*, 66(2):838–847, February 2018.
- [45] Gerardo Silva-Oelker, Carlos Jerez-Hanckes, and Patrick Fay. Study of w/HfO₂ grating selective thermal emitters for thermophotovoltaic applications. *Optics Express*, 26(22):A929, October 2018.
- [46] Jan Sokolowski and Jean-Paul Zolésio. Introduction to shape optimization. In *Introduction to Shape Optimization*, pages 5–12. Springer, 1992.
- [47] Manuel E. Solano, Muhammad Faryad, Peter B. Monk, Thomas E. Mallouk, and Akhlesh Lakhtakia. Periodically multilayered planar optical concentrator for photovoltaic solar cells. *Applied Physics Letters*, 103(19):191115, November 2013.
- [48] Gilbert Strang, editor. *Computational Science and Engineering*. Wellesley-Cambridge, 2007.
- [49] Sudheer, S. Porwal, S. Bhartiya, B. T. Rao, P. Tiwari, Himanshu Srivastava, T. K. Sharma, V. N. Rai, A. K. Srivastava, and P. A. Naik. Diffraction efficiency of plasmonic gratings fabricated by electron beam lithography using a silver halide film. *Journal of Applied Physics*, 120(4):043101, July 2016.
- [50] Leung Tsang, Jin Au Kong, Kung-Hau Ding, and Chi On Ao. *Scattering of Electromagnetic Waves: Numerical Simulations*. John Wiley & Sons, Inc., May 2001.
- [51] Joan Vila-Comamala, Lucia Romano, Vitaliy Guzenko, Matias Kagias, Marco Stampaoni, and Konstantins Jefimovs. Towards sub-micrometer high aspect ratio x-ray gratings by atomic layer deposition of iridium. *Microelectronic Engineering*, 192:19–24, May 2018.
- [52] Kang Wei and Yi Zhao. Fabrication of anisotropic and hierarchical undulations by benchtop surface wrinkling. In *2014 IEEE 27th International Conference on Micro Electro Mechanical Systems (MEMS)*. IEEE, January 2014.
- [53] R W Wood. On a remarkable case of uneven distribution of light in a diffraction grating spectrum. *Proceedings of the Physical Society of London*, 18(1):269–275, June 1902.
- [54] Zhaoning Yu, Lei Chen, Wei Wu, Haixiong Ge, and Stephen Y. Chou. Fabrication of nanoscale gratings with reduced line edge roughness using nanoimprint lithography. *Journal of Vacuum Science & Technology B: Microelectronics and Nanometer Structures*, 21(5):2089, 2003.
- [55] Uwe D. Zeitner, Maria Oliva, Frank Fuchs, Dirk Michaelis, Tino Benkenstein, Torsten Harzendorf, and Ernst-Bernhard Kley. High performance diffraction gratings made by e-beam lithography. *Applied Physics A*, 109(4):789–796, October 2012.
- [56] Bo Zhang and Simon N. Chandler-Wilde. Integral equation methods for scattering by infinite rough surfaces. *Mathematical Methods in the Applied Sciences*, 26(6):463–488, 2003.